Three-Dimensional Printing of Highly Stretchable and Tough Hydrogels into Complex, Cellularized Structures

DOI: 10.1002/((please add manuscript number))
Article type: Communication

Three-Dimensional Printing of Highly Stretchable and Tough Hydrogels into Complex, Cellularized Structures

*Sungmin Hong†, Dalton Sycks†, Hon Fai Chan†, Shaoting Lin, Gabriel P. Lopez, Farshid Guilak, Kam W. Leong, and Xuanhe Zhao**

Dr. S. Hong, D. Sycks, S. Lin, Prof. G. P. Lopez, Prof. F. Guilak, and Prof. X. Zhao
Department of Mechanical Engineering and Material Science, Duke University, Durham, NC 27708, USA
H. F. Chan, Prof. G. P. Lopez, Prof. F. Guilak, and Prof. K. W. Leong
Department of Biomedical Engineering, Duke University, Durham, NC 27708, USA
S. Lin and Prof. X. Zhao
Department of Mechanical Engineering, Massachusetts Institute of Technology, Cambridge, MA 02139, USA
Prof. F. Guilak
Department of Orthopaedic Surgery, Duke University Medical Center, Durham, NC 27710, USA
Prof. K. W. Leong
Department of Biomedical Engineering, Columbia University, New York, NY 10027; USA
Prof. X. Zhao
Department of Civil and Environmental Engineering, Massachusetts Institute of Technology, Cambridge, MA 02139, USA
E-mail: zhaox@mit.edu
† These authors contributed equally to this work.

While tough hydrogels are being intensively developed as robust scaffolds in biological research and biomedical engineering,[1-5] the application of these hydrogels is often severely limited by their incapability to encapsulate viable cells or form functional three-dimensional (3D) structures. Here, we report a new alginate-poly (ethylene glycol) hydrogel with designed, bimodal chain-length distributions and hybrid crosslinking that can achieve high stretchability (>500%), toughness (>1500 Jm^{-2}), and encapsulation of human mesenchymal stem cells (hMSCs) with high viability (>80%). Using biocompatible nanoclays to tune the viscosity of pre-gel solutions, we further print the tough and stretchable hydrogel into a wide variety of complex structures that

can act as a structural scaffold to host cells. Owing to its simple one-step synthesis and facile 3D printing, we expect the new hydrogel will find broad and important applications; for example, to develop cellularized constructs that can withstand high *in vivo* stretch, or to mechanically stimulate hMSCs at high strains in 3D hydrogel scaffolds *in vitro* or *in vivo* for controlled differentiation or tissue regeneration.

Living tissues usually have high fracture toughness in order to withstand substantial internal and external mechanical loads.[6] This challenges researchers to design hydrogels capable of achieving similar toughness in order to withstand physiological mechanical loads.[7] Despite recent success in developing tough hydrogels,[2, 3, 8-15] the fabrication of these hydrogels often involves toxic chemicals and/or harsh reactions, limiting their capability to encapsulate cells. In addition, it is desirable to fabricate cell-embedded hydrogels with macroporous architecture conducive to generation of complex tissues. While 3D printing offers rapid prototyping[16-20] and can print hydrogels into complex 3D structures for functions such as vascular networks[17, 19] and aortic valves,[21, 22] it has not been able to print tough hydrogels with complex geometry other than simple and flat structures such as dog-bone samples due to the difficulty of controlling pre-gel solutions' viscosity.[18]

Here, we chose the biocompatible materials sodium alginate and poly (ethylene glycol) (PEG) to constitute an interpenetrating network (**Figure 1**). The resultant hydrogel of covalently crosslinked PEG and ionically crosslinked alginate possesses high fracture toughness and allows cell encapsulation (**Figure 2** and **3**). (Detailed formulation of the hydrogel is described in the Experimental Section). We hypothesize that the toughening of this biocompatible hydrogel relies on a combination of two mechanisms: the reversible Ca^{2+} crosslinking of alginate dissipates mechanical energy, while the covalently crosslinking of PEG maintains elasticity under large

deformations (Figure 1). To test this hypothesis, we varied the molecular weight of PEG (6,000 Da to 20,000 Da) and the concentrations of Ca^{2+} (25 µl of either 0M or 1M $CaSO_4$ solution added per 1 mL of the pre-gel PEG-alginate mixture) in the hydrogels, and used pure-shear tests to measure the fracture energies of the resultant hydrogels.[23] (Details of the pure-shear test are described in **Figure S1**). As shown in **Figure S2**a, the fracture energies of hydrogels without Ca^{2+} are consistently low (below 211 Jm^{-2}) and they display negligible stress-strain hysteresis (Figure S2b). Introducing reversible Ca^{2+} crosslinking into the hydrogels significantly increases their fracture energies. The increase in fracture energy is also accompanied by significant increase in stress-strain hysteresis, which indicates mechanical dissipation in the hydrogels under deformation (Figure S2b). In addition, the fracture energy of calcium-containing hydrogels increases drastically with the molecular weight of PEG, because the longer polymer chains of PEG allow for higher stretchability of the hydrogel (Figure S2a and c). These results validate the hypothesis that the combined mechanisms of mechanical energy dissipation and high elasticity are critical to the toughening of the PEG-alginate hydrogels. To further test the hypothesis, we made a set of pure PEG hydrogels with different molecular weights and concentrations of PEG and measured their fracture energies. From Figure S2a and S3, it is evident that the fracture energies of pure PEG hydrogels are significantly lower than the corresponding PEG-alginate hydrogels with Ca^{2+}, further validating the proposed toughening mechanism.

By further optimizing the concentrations of polymers and photo initiators (**Figure S3** and **S4**), the resultant hydrogel with 20 wt % PEG and 2.5 wt % alginate can reach a maximum fracture energy of ~1,500 Jm^{-2}, which is higher than the value of articular cartilage.[24] Furthermore, we used a digital image correlation technique[25] to measure the stress field around the tip of a crack in the hydrogel under pure shear tests. (Details of the digital image correlation technique are described in the Experimental Section and in **Figure S5**). As shown in Figure 2a,

the crack in the hydrogel becomes highly blunted and the principal stress/strain at the crack tip before crack propagation reaches approximately the ultimate tensile strength/strain of the same, unnotched hydrogel under pure-shear tension (Figure 2b). This indicates that the alginate-PEG hydrogel is indeed a tough, soft material.[26]

In addition, since the mechanical energy dissipation in the PEG-alginate hydrogel relies on reversible crosslinking, the dissipative property of the hydrogel is partially recoverable after deformation.[2] We illustrated this point by stretching a hydrogel sample with the optimized composition to a strain of 400%, followed by relaxation of the sample. The relaxed sample was then kept in a humid chamber at 37 ˚C, and we repeated the stretch-relax tests after 30 minutes and 24 hours of storage. Figure 2c shows that after storage at 37 ˚C for 24 hours, the deformed hydrogel can achieve 58.9% of the hysteresis in the first loading-unloading cycle, indicating partial recovery of the dissipative properties due to reversible crosslinking of Ca^{2+}.

The recovery of ionic crosslinking responsible for energy dissipation contributes to the maintenance of relatively high fracture energy of the hydrogel after deformation.[1, 2] To demonstrate this, we stretched a set of hydrogels to different strains, ranging from 0% to 500%, under uniaxial tension. The fracture energies of the pre-deformed hydrogels were measured either right after the pre-strain or after storage in a humid chamber at 37 ˚C for 24 h. The measured fracture energies of hydrogels under different pre-strains are given in Figure 2d. It can be seen that pre-strained hydrogels have drastically reduced fracture energies if tested immediately after deformation, since the dissipative ionic crosslinks do not have enough time to reform. On the other hand, if pre-strained hydrogels are stored at 37 ˚C for 24 hours, they can recover most of their high fracture energy. For example, a hydrogel subjected to a large strain of 500% and then stored at 37 ˚C for 24 hours recovered 70.5% of the fracture energy of the undeformed gel. Such

retention of fracture toughness after deformation is critical to the design of anti-fatigue hydrogels.[3, 9]

Both PEG and alginate are widely known to be biocompatible and have been extensively used in biomedical applications.[27, 28] We hypothesized that the tough PEG-alginate hydrogel can be used to encapsulate cells while maintaining high viability of the encapsulated cells for biomedical applications. To test this hypothesis, human mesenchymal stem cells (hMSCs) encapsulated in the hydrogels were monitored for viability. Before encapsulation, 2 mL of PEG-alginate mixture was prepared, and the hMSC suspension was centrifuged at 1000 rpm for 5 minutes. The cell pellet was re-suspended with 70 μL of I-2959 (1%, w/vol in H_2O) and mixed with PEGDA-alginate solution to seed a final cell density of 3×10^6 cells/mL. Then, 50 μL of $CaSO_4\cdot 2H_2O$ slurry was thoroughly mixed into the hydrogel, which was then transferred to a glass mold and exposed to 365 nm UV light for 10 minutes to crosslink the solution into PEG-alginate hydrogel. The hydrogel was immersed in α-minimum essential medium with 20% fetal bovine serum and 1% penicillin/streptomycin. Live/dead assays were used to determine cell viability in the hydrogel over the course of 7 days. From Figure 3a, it can be seen that high cell viability, ranging from 86.0 ± 3.8% to 75.5 ± 11.6%, was maintained over seven days of culture. The result indicates that the current synthesis of the PEG-alginate hydrogel is a benign, cell-friendly process and the resultant hydrogel allows for nutrient diffusion and waste transport to support viable cell culture over extended periods of time.

Because the PEG-alginate hydrogel is highly stretchable and tough, the hMSCs encapsulated in this 3D extracellular matrix can be highly deformed by stretching the hydrogel. To illustrate this point, the hydrogel with encapsulated hMSCs was stretched to various strains from 0% to 300%, and then fixed on a clean glass slide. The stretched gels were imaged under a Zeiss LSM 510 inverted confocal laser microscope. As shown in Figure 3b, both the actin-

filament network and nuclei are highly deformed together with the gel. Consequently, the ratio between two axes of cell bodies and nuclei drastically increased with applied strains, as shown in Figure 3c.

Next, we demonstrate the capability of printing the PEG-alginate hydrogels into various complicated 3D structures that can also be cellularized. Controlling the viscosity of the pre-gel solution is critical to the success of printing 3D structures of hydrogels.[17, 18, 29] It is usually desirable for the pre-gel solution to have relatively low viscosity at high shear rate but much higher viscosity at low shear rate, so that the pre-gel solution can easily flow out of the printer but maintain its shape once printed.[21, 22, 30] Here, we chose to use bio-compatible nanoclay (Laponite XLG, BYK Additives, Inc., TX) to control the viscosity of the pre-gel solution[31] by incorporating it into the PEG/alginate hydrogel. The nanoclay particles physically crosslink both with themselves, as well as with the polymer networks of the PEG and alginate to increase the viscosity of the pre-gel solution.[32, 33] A cone and plate rheometer (TA Instruments, New Castle, DE) was used to confirm the increase in viscosity of the pre-gel solution as a function of nanoclay content, while maintaining its ability to shear thin and flow under the high shear rates present in the extrusion needle (**Figure S6**).

Because nanoclay significantly enhances the viscosity of the pre-gel solution and also increases its shear-thinning properties, we chose the PEG-alginate-nanoclay system as the ink of our 3D printer (Fab@Home Model 3, Seraph Robotics, Inc., NY). The printing process is described in the Methods section. In **Figure 4**a **and Supplementary Movie 1**, we show that the PEG-alginate-nanoclay hydrogels can be printed into diverse shapes such as a hollow cube, hemi-sphere, pyramid, twisted bundle and physiologically-relevant shapes such as human nose and ear models. Printed objects may also be composed of multiple materials, which is illustrated in the two-color mesh in Figure 4b. The mesh consists of alternating layers of PEG-alginate-nanoclay

that either contains red or green food dye to demonstrate this concept. The spatial resolution of the printed objects depends on factors such as precision of the printer, the pre-gel viscosity and extrusion needle diameter, and is approximately 500 µm with the current printer. This resolution is consistent with previous reports on hydrogel structures printed with the same type of printer (i.e., Fab@Home) [21, 22]. Tough hydrogel structures of higher resolution may be achieved by using the PEG-alginate-nanoclay system with a 3D printer of higher precision.

To investigate the biocompatibility of the printed tough hydrogel with incorporated nanoclay, human embryonic kidney (HEK) cells were encapsulated into a type 1 rat tail collagen solution (Corning Inc., Corning, NY), which then gelled throughout the interconnected pores of the printed PEG-alginate-nanoclay mesh to form a composite hydrogel (**Figure S7**). The encapsulated HEK cells were seeded at a concentration of 3×10^6 cells/mL of collagen gel, and maintained high viability (~95%) over the course of 7 days of culture (Figure 4c and 4d).

The printed hydrogel structures are also highly deformable and tough, demonstrating that the added nanoclay does not significantly affect the superior mechanical qualities of the hydrogel. As shown in Figure 4e, a printed mesh of the hydrogel was uniaxially stretched to 300% of its undeformed length, held for one minute, and allowed to relax to its initial state. The mesh experienced very little permanent deformation, since the long-chain PEG network maintains the high elasticity of the hydrogel. Figure 4f and **Supplementary Movie 2** show a printed pyramid that undergoes 99% compressive strain and regains 97% of its original height within 5 minutes of unloading.

In conclusion, we have created a tough hydrogel comprised of PEG and sodium alginate that can be used for cell encapsulation. The hydrogel can endure high stress in both tension and compression and has a fracture toughness above 1,500 Jm^{-2}, making it tougher than natural cartilage and yet with water content (~77.5 wt %) that is tunable and within the physiologically

acceptable range. The reversible crosslinking of the alginate dissipates mechanical energy under deformation and the long-chain PEG network maintains high elasticity of the hydrogel; these phenomena combine to result in a robust, tough hydrogel. Encapsulated cells showed high viability over 7 days, averaging 75.5 ± 11.6% in the PEG-alginate hydrogel and 95% in infiltrated collagen between the pores of a printed PEG-alginate-nanoclay mesh. In addition, we were able to print the tough hydrogel into complicated 3D structures by using nanoclay to control the pre-gel solution's viscosity. To our knowledge, this study is the first to demonstrate a hydrogel that is not only tough and 3D-printable, but suitable for long-term cell culture as well.

Experimental Section

PEG-alginate hydrogel fabrication: PEG powder was purchased from Sigma Aldrich and modified into poly (ethylene glycol) diacrylate (PEGDA) according to previously published protocols[34] and dissolved in deionized water (DI, 40 wt %). Brown sodium alginate solution (5 wt %) was mixed with 40% PEGDA solution. After degassing the solution in a vacuum chamber, Irgacure 2959 (I-2959) and calcium sulfate slurry (1M $CaSO_4 \cdot 2H_2O$) were added as photo initiator for PEGDA and ionic crosslinker for alginate, respectively. The mixture was then carefully poured into a glass mold and cured under ultraviolet light (365nm wavelength) for 10min. PEGDA chains covalently crosslink via radicals generated from the photo initiator (I-2959) when exposed to UV and form a covalent, ductile network capable of large deformation. In contrast, alginate is ionically crosslinked in the presence of divalent cations (such as Ca^{2+}) and imparts stiffness into the network. These ionic bonds reversibly form, break, and reform in the hydrogel's aqueous environment and enable fast recovery after deformation. As the network is stretched, the ionically crosslinked alginate chains release entrapped divalent cations and dissipate applied mechanical energy while covalently crosslinked PEGDA elastically deforms in

the direction of the load. When the hydrogel is released from stress, alginate recovers its crosslinking by recombining the calcium cations. After curing, mechanical tests were performed at room temperature using a dynamic mechanical analyzer (RSA III, TA instruments, DE).

Digital image correlation: As is illustrated by Figure S5, digital image correlation is a non-contact optical technique that allows full-field strain measurement on a surface under deformation.[35] A random speckle pattern was generated on the surface of a sample via spray painting. Images of speckle patterns at both the reference state and deformed state were recorded by a standard video camera during the process of the deformation. Based on the video, the commercial software VIC-2D (Correlated Solutions Inc., Columbia, SC) was applied to measure strain mapping of the deformed sample. Essentially, both images were transformed to grayscale matrices. To track the surface displacements of deforming materials, a mathematically well-defined correlated function was applied to match digitalized images before deformation and after deformation:

$$r(x,y) = 1 - \frac{\sum A(x,y)B(x^*,y^*)}{(\sum A(x,y)^2 * \sum B(x^*,y^*)^2)^{1/2}}$$

$A(x,y)$ is the gray level at the location of (x,y) at reference state, $B(x^*,y^*)$ represents the gray level at the location of (x^*,y^*) at deformed state. The relation between (x^*,y^*) and (x,y) can be related as:

$$\begin{cases} x^* = x + u + \dfrac{\partial u}{\partial x}\Delta x + \dfrac{\partial u}{\partial y}\Delta y \\ y^* = y + v + \dfrac{\partial v}{\partial x}\Delta x + \dfrac{\partial v}{\partial y}\Delta y \end{cases}$$

Where u and v respectively represents the displacements in the direction of x and y .The displacements can be determined by minimizing the correlation function $r(x,y)$.

Cell culture: Bone-marrow-derived hMSCs were provided by Tulane University Health Sciences Centre and cultured in α-minimum essential medium supplemented with 20% fetal bovine serum and 1% penicillin/streptomycin at 37 °C and 5% CO_2. The 4–7th passages of hMSCs were used in this study. HEK-293 cell line was obtained from ATCC (Manassas, VA) and cultured in Dulbecco's modified eagle medium (high glucose) with 10% fetal bovine serum and 1% penicillin/streptomycin. Cells were trypsinized with 0.25% Trypsin-EDTA (Life Technologies, Grand Island, NY) before being counted and mixed with the gel precursor solution.

Viability test: To perform viability testing, the samples were washed in 1X Dulbecco's phosphate buffered saline before soaking in 2μM Calcein AM (Sigma-Aldrich, St. Louis, MO) and 5μM propidium iodide (Sigma-Aldrich, St. Louis, MO) solution for 30 min. Fluorescent images were taken using Zeiss LSM 510 inverted confocal microscope provided by Duke University Light Microscopy Core Facility.

Collagen gel preparation for cell encapsulation: Type 1 rat tail collagen (Corning Inc., Corning, NY) was diluted with 0.6% acetic acid (Sigma-Aldrich, St. Louis, MO) to a final collagen concentration of 2mg/ml. This solution was neutralized with 5M NaOH (Sigma-Aldrich, St. Louis, MO), and 10X α-minimum essential media (Sigma-Aldrich, St. Louis, MO) was added to a final concentration of 1X. HEK cells were added, and the solution formed a gel over the course of 30 minutes of incubation at room temperature.

Cell staining for stretch testing: The samples were fixed with 4% paraformaldehyde (Electron Microscopy Sciences, Hatfield, PA) for 30 min before staining with Alexa Fluor® 488 Phalloidin for the actin-filament network (Life Technologies, Grand Island, NY) and DAPI for the nucleus (Sigma-Aldrich, St. Louis, MO) for 1 hour. The samples were washed with PBS for three times before being mounted on a glass slide for imaging.

3D Printing PEG-alginate-nanoclay hydrogel: PEGDA–alginate mixture was prepared as described above, but Laponite XLG (final concentration 5 wt %) was first dissolved into deionized water, followed by PEGDA. This gel was allowed to homogenize and settle overnight, after which it was mixed in a 1:1 ratio with the 5 wt% alginate solution and allowed to equilibrate for one additional day. After degassing, I-2959 and $CaSO_4$ solution were added to the pre-gel solution. The PEGDA-alginate-nanoclay pre-gel solution was then loaded into extrusion cartridges, which were placed on the printing carriage of 3D printer for extrusion through a 15G-20G flat tip needle. During printing, the pre-gel solution experienced shear thinning inside the extrusion needle, and quickly regained its viscosity upon exiting. Following extrusion, the flat printed shapes were encased in glass slides and placed in the UV chamber to complete covalent crosslinking of the PEGDA polymer chains. Three-dimensional shapes were crosslinked in a sealed, nitrogenous environment under a $100mWcm^{-2}$ UV source with emission peaks centered on 365nm. Since the viscosity of hydrogel was enhanced by adding nanoclay, it was able to be printed into various shapes free from vertical limitation (Figure 4a). Controlling the concentration of nanoclay in the gel permits the viscosity to be optimized for extrusion-based printing while still maintaining three dimensional structures without requiring support material (Figure S4).

Supporting Information

Supporting Information is available from the Wiley Online Library or from the author.

Acknowledgements

The work was supported by NIH grants (UH3TR000505 and R01AR48825) and the NIH Common Fund for the Microphysiological Systems Initiative, ONR grants (N00014-14-1-0619 and N0014-13-1-0828), AOSpine Foundation, and NSF Triangle MRSEC (DMR-1121107). D.S. acknowledges support by the National Science Foundation Graduate Research Fellowship under Grant No. 1106401. The authors gratefully acknowledge Ha Yeun Ji for her help with cell viability experiments.

Received: ((will be filled in by the editorial staff))
Revised: ((will be filled in by the editorial staff))
Published online: ((will be filled in by the editorial staff))

[1] J. P. Gong, Y. Katsuyama, T. Kurokawa, Y. Osada, Advanced Materials 2003, 15, 1155.
[2] J.-Y. Sun, X. Zhao, W. R. K. Illeperuma, O. Chaudhuri, K. H. Oh, D. J. Mooney, J. J. Vlassak, Z. Suo, Nature 2012, 489, 133.
[3] T. L. Sun, T. Kurokawa, S. Kuroda, A. B. Ihsan, T. Akasaki, K. Sato, M. A. Haque, T. Nakajima, J. P. Gong, Nat Mater 2013, 12, 932.
[4] H. Yin, T. Akasaki, T. Lin Sun, T. Nakajima, T. Kurokawa, T. Nonoyama, T. Taira, Y. Saruwatari, J. Ping Gong, Journal of Materials Chemistry B 2013, 1, 3685.
[5] M. A. Haque, T. Kurokawa, J. P. Gong, Polymer 2012, 53, 1805.
[6] D. Taylor, N. O'Mara, E. Ryan, M. Takaza, C. Simms, Journal of the Mechanical Behavior of Biomedical Materials 2012, 6, 139.
[7] B. O. Diekman, N. Christoforou, V. P. Willard, H. Sun, J. Sanchez-Adams, K. W. Leong, F. Guilak, Proceedings of the National Academy of Sciences 2012, 109, 19172.
[8] C. M. Hassan, N. A. Peppas, Macromolecules 2000, 33, 2472.
[9] X. Zhao, Soft Matter 2014, 10, 672.
[10] I. C. Liao, F. T. Moutos, B. T. Estes, X. Zhao, F. Guilak, Advanced functional materials 2013, 23, 5833.
[11] J. Yang, C.-r. Han, F. Xu, R.-c. Sun, Nanoscale 2014, 6, 5934.
[12] S. Lin, C. Cao, Q. Wang, M. Gonzalez, J. E. Dolbow, X. Zhao, Soft matter 2014, 10, 7519.
[13] J. Yang, C.-R. Han, X.-M. Zhang, F. Xu, R.-C. Sun, Macromolecules 2014, 47, 4077.
[14] J. Li, Z. Suo, J. J. Vlassak, J. Mater. Chem. B 2014, 2, 6708.
[15] S. Lin, Y. Zhou, X. Zhao, Extreme Mechanics Letters, http://dx.doi.org/10.1016/j.eml.2014.11.002.
[16] N. E. Fedorovich, J. Alblas, J. R. de Wijn, W. E. Hennink, A. J. Verbout, W. J. Dhert, Tissue engineering 2007, 13, 1905.
[17] D. B. Kolesky, R. L. Truby, A. S. Gladman, T. A. Busbee, K. A. Homan, J. A. Lewis, Advanced Materials 2014, 26, 3124.
[18] S. E. Bakarich, M. i. h. Panhuis, S. Beirne, G. G. Wallace, G. M. Spinks, Journal of Materials Chemistry B 2013, 1, 4939.
[19] J. S. Miller, K. R. Stevens, M. T. Yang, B. M. Baker, D.-H. T. Nguyen, D. M. Cohen, E. Toro, A. A. Chen, P. A. Galie, X. Yu, R. Chaturvedi, S. N. Bhatia, C. S. Chen, Nat Mater 2012, 11, 768.
[20] R. A. Barry, R. F. Shepherd, J. N. Hanson, R. G. Nuzzo, P. Wiltzius, J. A. Lewis, Advanced materials 2009, 21, 2407.
[21] B. Duan, L. A. Hockaday, K. H. Kang, J. T. Butcher, Journal of Biomedical Materials Research Part A 2013, 101A, 1255.
[22] L. A. Hockaday, K. H. Kang, N. W. Colangelo, P. Y. Cheung, B. Duan, E. Malone, J. Wu, L. N. Girardi, L. J. Bonassar, H. Lipson, C. C. Chu, J. T. Butcher, Biofabrication 2012, 4, 035005.
[23] R. S. Rivlin, A. G. Thomas, Journal of Polymer Science 1953, 10, 291.
[24] N. K. Simha, C. S. Carlson, J. L. Lewis, Journal of Materials Science: Materials in Medicine 2004, 15, 631.

[25] H. A. Bruck, S. R. McNeill, M. A. Sutton, W. H. Peters, III, Experimental Mechanics 1989, 29, 261.
[26] C. Y. Hui, J. A, S. J. Bennison, J. D. Londono, Proceedings of the Royal Society of London A: Mathematical, Physical and Engineering Sciences 2003, 459, 1489.
[27] C. Fan, L. Liao, C. Zhang, L. Liu, Journal of Materials Chemistry B 2013, 1, 4251.
[28] A. D. Rouillard, C. M. Berglund, J. Y. Lee, W. J. Polacheck, Y. Tsui, L. J. Bonassar, B. J. Kirby, Tissue engineering. Part C, Methods 2011, 17, 173.
[29] S. Khalil, J. Nam, W. Sun, Rapid Prototyping Journal 2005, 11, 9.
[30] R. Chang, J. Nam, W. Sun, Tissue engineering. Part A 2008, 14, 41.
[31] C.-W. Chang, A. van Spreeuwel, C. Zhang, S. Varghese, Soft Matter 2010, 6, 5157.
[32] P. C. Thomas, B. H. Cipriano, S. R. Raghavan, Soft Matter 2011, 7, 8192.
[33] J. Wang, L. Lin, Q. Cheng, L. Jiang, Angewandte Chemie International Edition 2012, 51, 4676.
[34] S. Nemir, H. N. Hayenga, J. L. West, Biotechnology and bioengineering 2010, 105, 636.
[35] W. H. Peters, W. F. Ranson, OPTICE 1982, 21, 213427.

Figures and Figure Captions

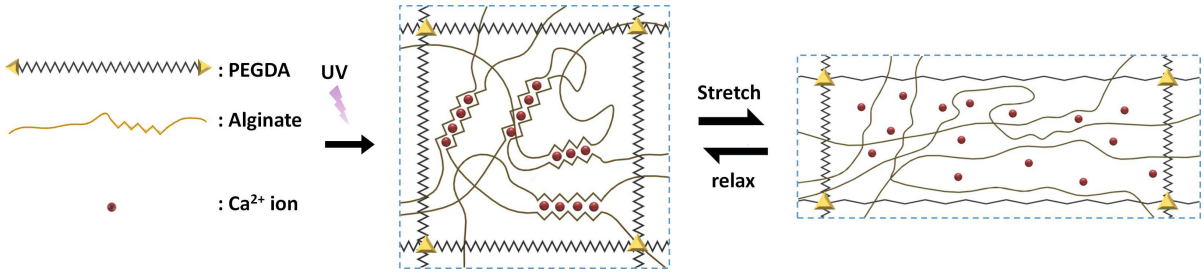

Figure 1. Schematic diagrams of the biocompatible and tough hydrogel. PEG and alginate polymers are covalently and ionically crosslinked through UV exposure and Ca^{2+}, respectively. As the hydrogel is deformed, the alginate chains are detached from the reversible ionic crosslinks and mechanical energy is dissipated. Once the hydrogel is relaxed from deformation, it regains its original configuration since the covalently crosslinked PEG network maintains the elasticity of the hydrogel. Over time, some of the ionic crosslinks in the alginate network can reform in the deformed and relaxed hydrogel.

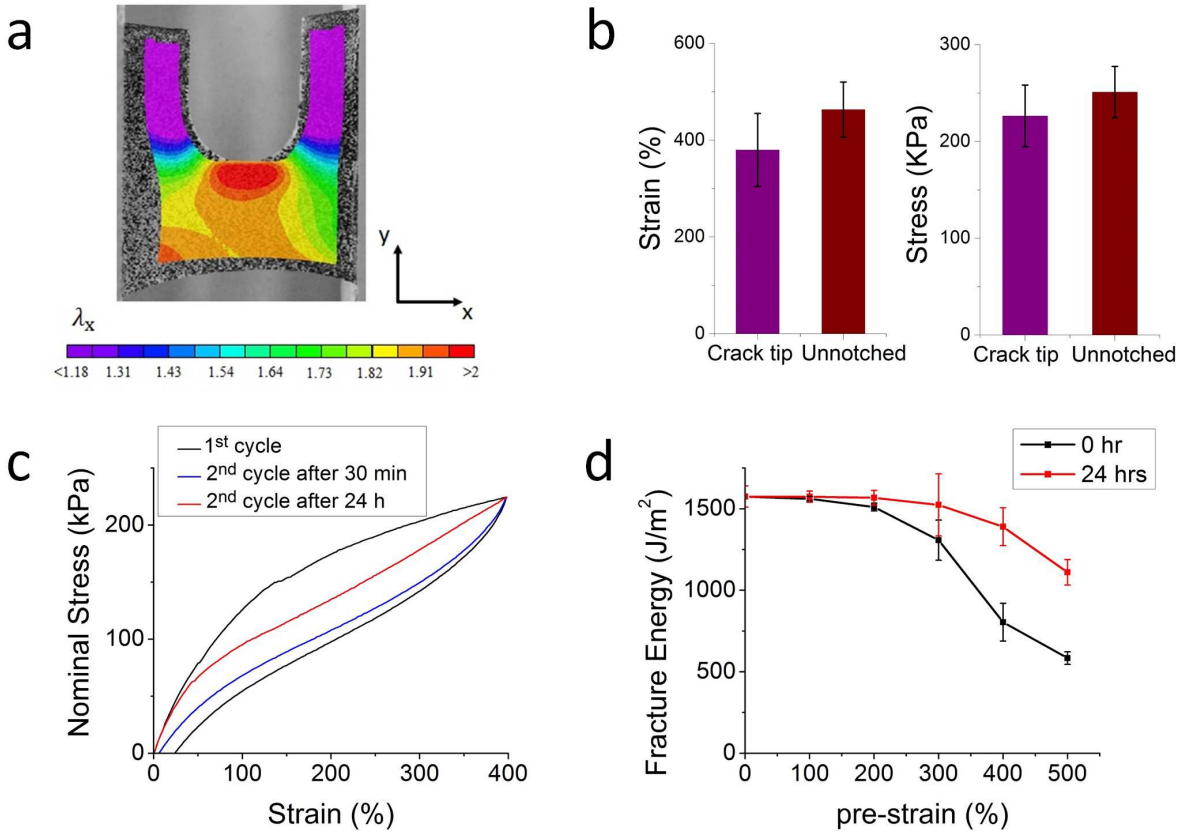

Figure 2. . Mechanical properties of the hydrogel. **a,** stretch along x-direction in a notched sample of the hydrogel under pure-shear test. **b.** comparison of the critical strain and stress at the crack tip before crack propagation and the failure strain and stress of a sample without notch under pure-shear tension. **c.** stress-strain hysteresis of the hydrogel under the first and second cycles of deformation. The sample was stored in a humid chamber at 37 ˚C for 5 min or 24 h between the two cycles of deformation. **d.** fracture energies of hydrogels pre-deformed to different strains. The fracture energies were measured right after the pre-deformation or after storing the hydrogel in a humid chamber at 37 ˚C for 24 h.

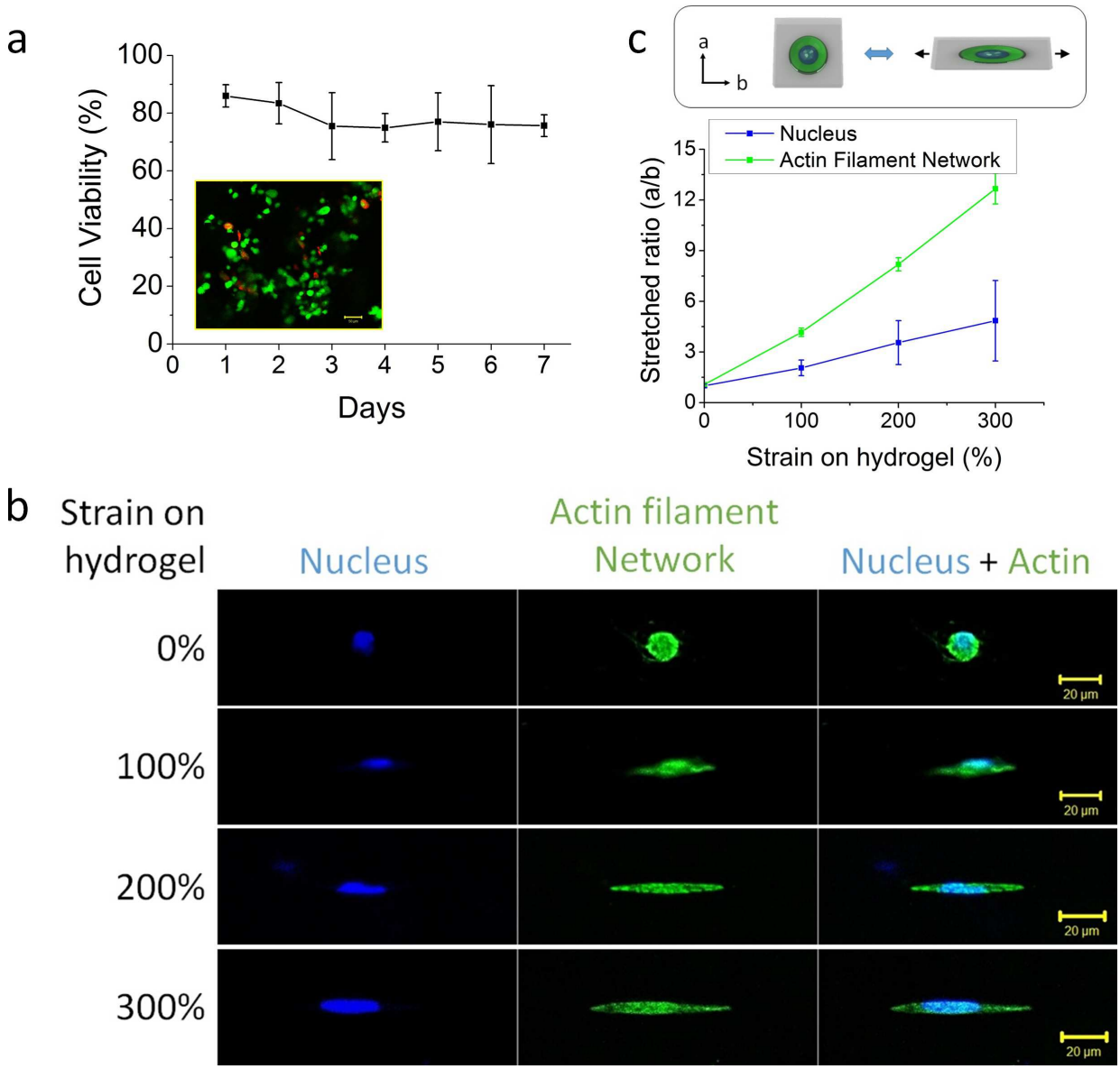

Figure 3. hMSC encapsulation in the hydrogel. **a,** hMSC viability results over 7 days (inset: Live/dead assay images after 7 days from encapsulation). **b,** deformation of the hMSC encapsulated in the hydrogel matrix, which was stretched to different strains. **c,** ratio of nucleus and cell body as a function of the applied strain on the hydrogel matrix.

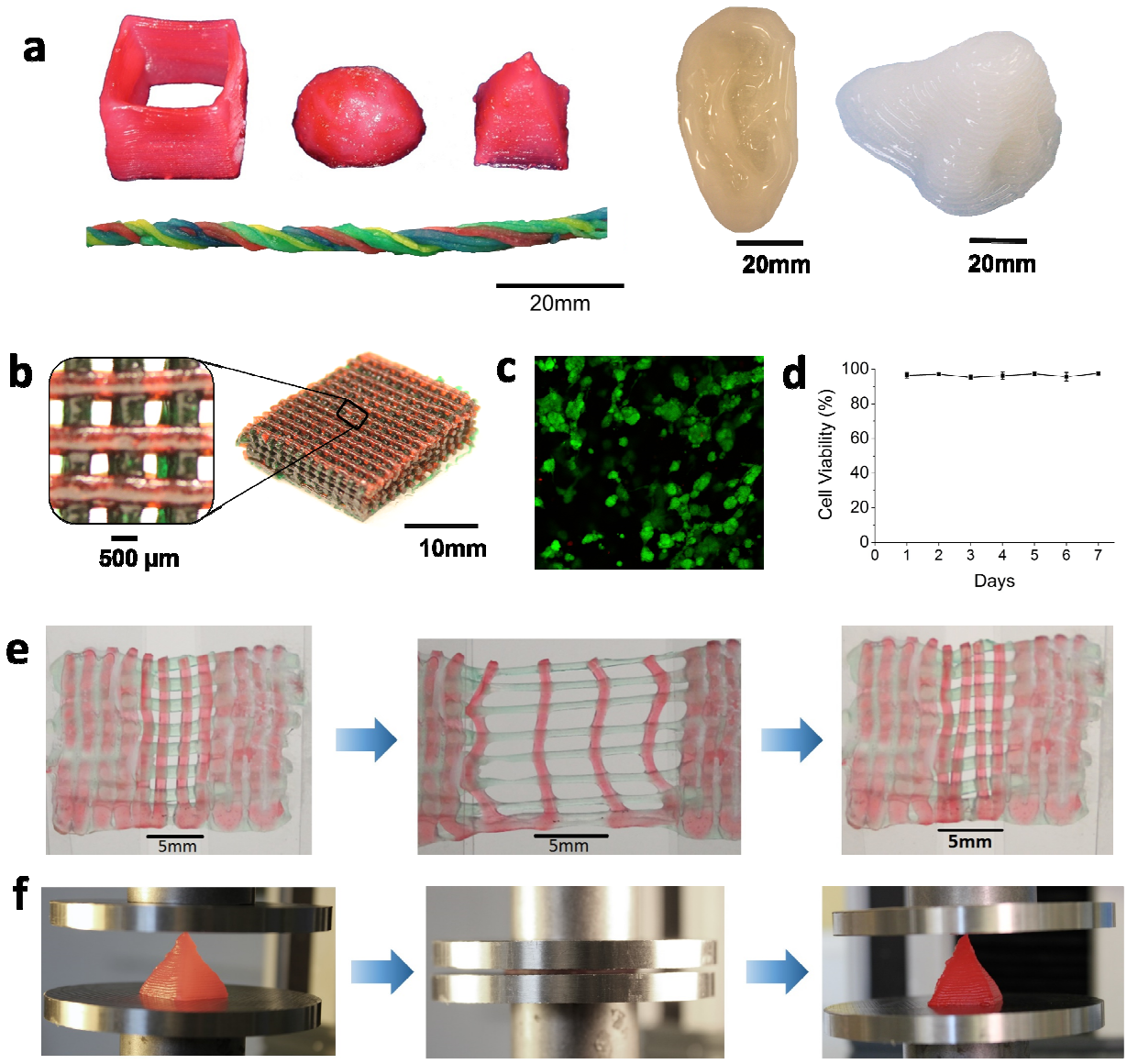

Figure 4. 3D printing of tough and biocompatible PEG-Alginate-nanoclay hydrogels. **a,** various three-dimensional constructs printed with the hydrogel (from left to right: hollow cube, hemi-sphere, pyramid, twisted bundle, the shape of an ear, and a nose. Non-toxic red food dye was added post-print on some samples for visibility). **b,** a mesh printed with the tough and biocompitable hydrogel. The mesh was used to host HEK cells **c,** live-dead assay of HEK cells in a collagen hydrogel infused into the 3D printed mesh of the PEG-Alginate-nanoclay hydrogel. **d,** viability of the HEK cells through 7 days. **e,** a printed bilayer mesh (top layer red, bottom layer green) is uniaxially stretched to three times of its initial length. Relaxation of the sample after stretching shows almost complete recovery of its original shape. **f,** a printed pyramid undergoes a compressive strain of 99% while returning to its original shape after relaxation.

A 3D printable and highly stretchable tough hydrogel is developed by combining PEG and sodium alginate, which synergize to form a hydrogel tougher than natural cartilage. Encapsulated cells maintain high viability over 7 days culture period and are highly deformed together with the hydrogel. By adding biocompatible nanoclay, the tough hydrogel is 3D printed various shape without requiring support material.

Sungmin Hong[†], Dalton Sycks[†], Hon Fai Chan[†], Shaoting Lin, Gabriel P. Lopez, Farshid Guilak,

Kam W. Leong, and Xuanhe Zhao[*]

Three-Dimensional Printing of Highly Stretchable and Tough Hydrogels into Complex, Cellularized Structures

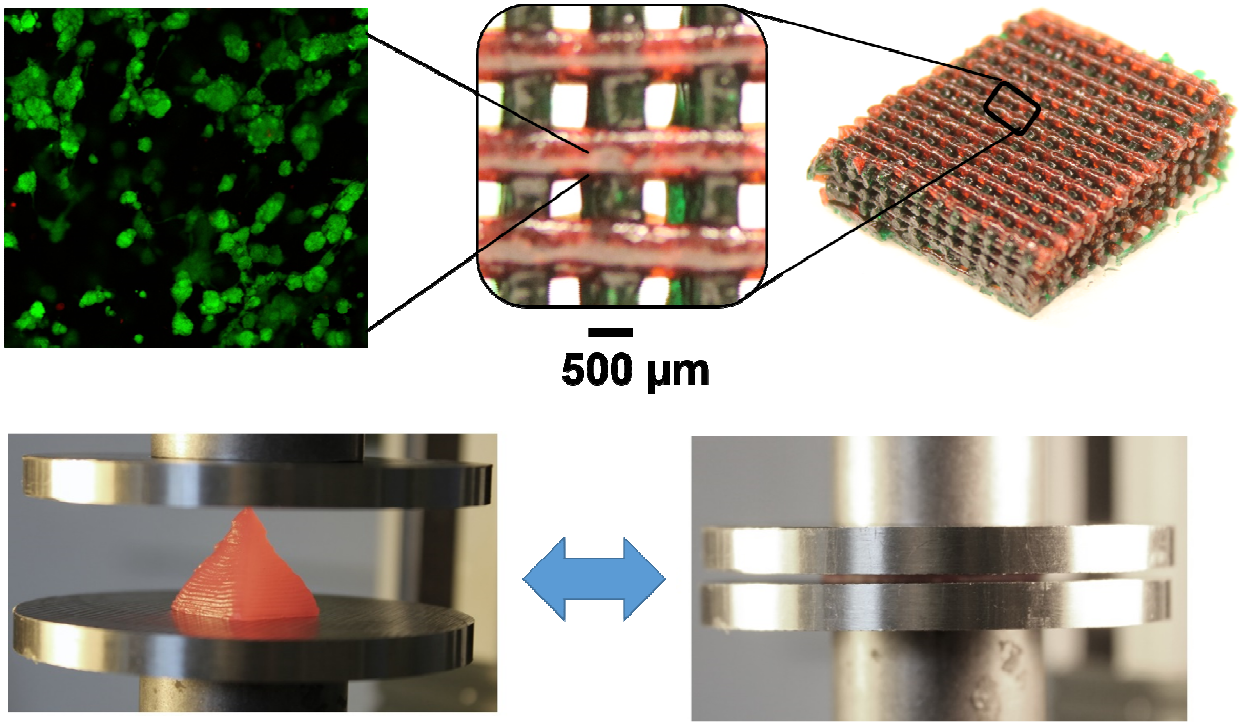

Supporting Information

Three-Dimensional Printing of Highly Stretchable and Tough Hydrogels into Complex, Cellularized Structures

*Sungmin Hong†, Dalton Sycks†, Hon Fai Chan†, Shaoting Lin, Gabriel P. Lopez, Farshid Guilak, Kam W. Leong, and Xuanhe Zhao**

Fracture energy of the hydrogel measured with the pure-shear test

A pure-shear test was used to measure the fracture energy of the hydrogel. As illustrated in **Figure S1,** we separately stretched two identical samples with the same thickness T_0, width W_0, and initial gauge length L_0, where $W_0 >> L_0 >> T_0$. One sample was notched with a crack with length of $\sim 0.5W_0$ and the other was un-notched. The notched sample was stretched to a critical distance L_c (length at which crack propagation began), while the un-notched sample was stretched to measure the force-displacement curve. The fracture energy of the gel can be calculated by $\Gamma = \frac{\int_{L_0}^{L_c} Fdl}{W_0 T_0}$.

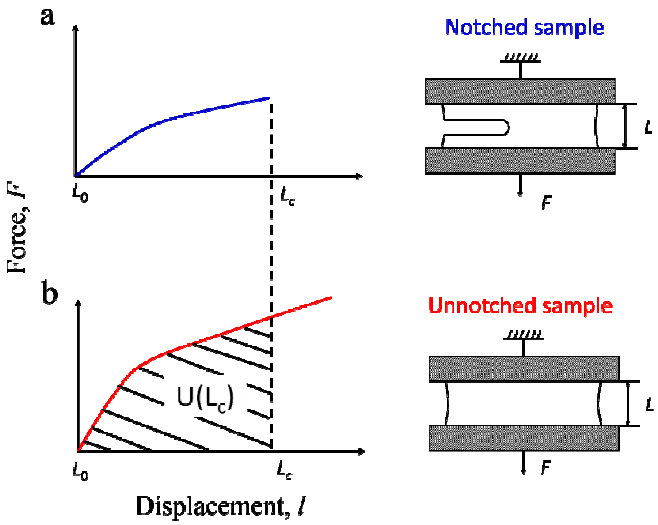

Figure S1. Schematic of the pure-shear test for measuring fracture energy of hydrogels. **a,** notched samples are stretched to a critical distance L_c, at which point crack propagation occurs; **b,** un-notched samples are stretched to L_c, with the force F recorded and the fracture energy of the hydrogel calculated as $\Gamma = (\int_{L_0}^{L_c} Fdl)/(W_0 T_0)$, where W_0, T_0 and L_0 represents width, thickness and initial gauge length of the sample, respectively.

Effect of Ca^{2+} and molecular weight of PEG on fracture energy and hysteresis

Mechanical properties were measured for PEG-alginate hydrogels with PEG of various molecular weights with or without Ca^{2+}. Each molecular weight of PEG (6,000, 10,000, or 20,000 Da, all held at 20 wt%) was mixed with the same concentration of alginate (2.5 wt%) and crosslinked under 365nm UV for 10 min.

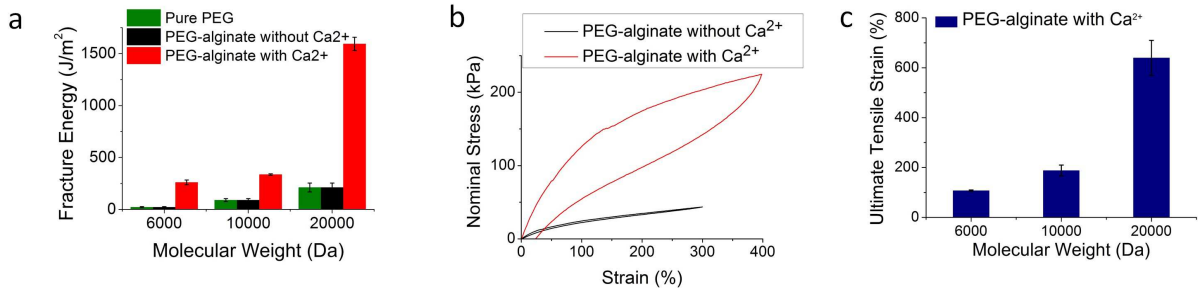

Figure S2. a, Comparison of fracture energies of PEG-alginate hydrogels without and with Ca^{2+} (50µl of 1M $CaSO_4 \cdot 2H_2O$ per 2mL of pre-gel solution) and pure PEG hydrogels as a function of molecular weight of PEG. **b,** stress-strain hysteresis loop of 20 kDa PEG-alginate hydrogel with and without Ca^{2+}. **c**, ultimate tensile strain as a function of PEG molecular weight.

Fracture energy of the hydrogel as a function of PEG concentration

The effect of PEG concentration on fracture energy of the hydrogel was investigated. Various concentrations of PEG-diacrylate (molecular weight 20,000Da) were mixed with a fixed concentration of alginate (2.5 wt%) in the pre-gel solutions. As shown in **Figure S3**, higher concentrations of PEG increase the fracture energy of the hydrogel. We chose 20 wt% PEG for the pre-gel solutions of PEG-alginate hydrogels in the current study, since the corresponding hydrogel readily exhibits fracture energy values surpassing 1,000 Jm^{-2}. As a control study, we also measured the fracture energy of hydrogels made from PEG-diacrylate (molecular weight 20,000Da) without alginate.

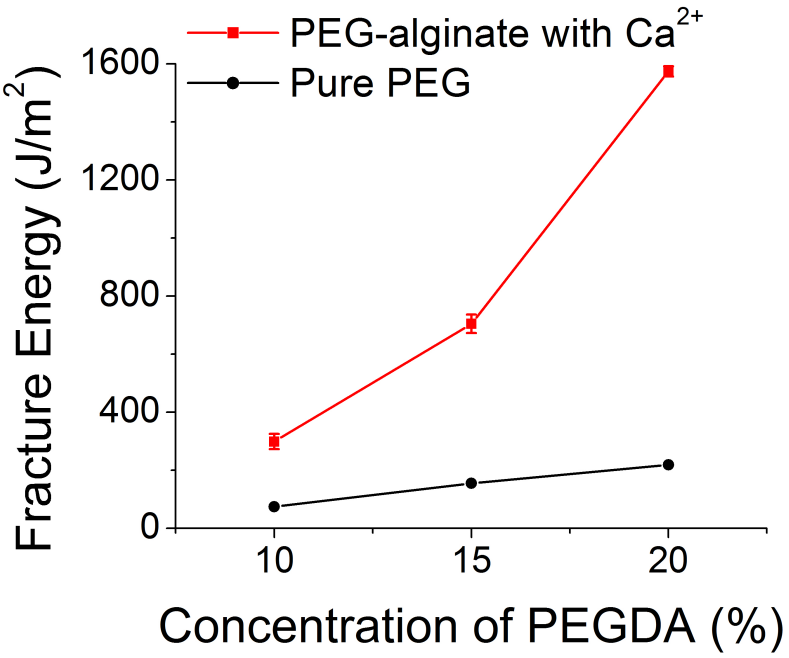

Figure S3. Fracture energy as a function of PEGDA concentration in the pre-gel solution.

Effect of photo initiator density on the fracture energy of PEG-alginate hydrogel

Various concentrations of photo initiator (I-2959) were mixed in the PEGDA-alginate pre-gel solutions. The concentration of 20 kDa PEGDA and alginate was fixed to be 20 wt% and 2.5 wt%, respectively. The fracture energy of the resultant PEG-alginate hydrogel varies with the concentration of I-2959 as shown in **Figure S4**.

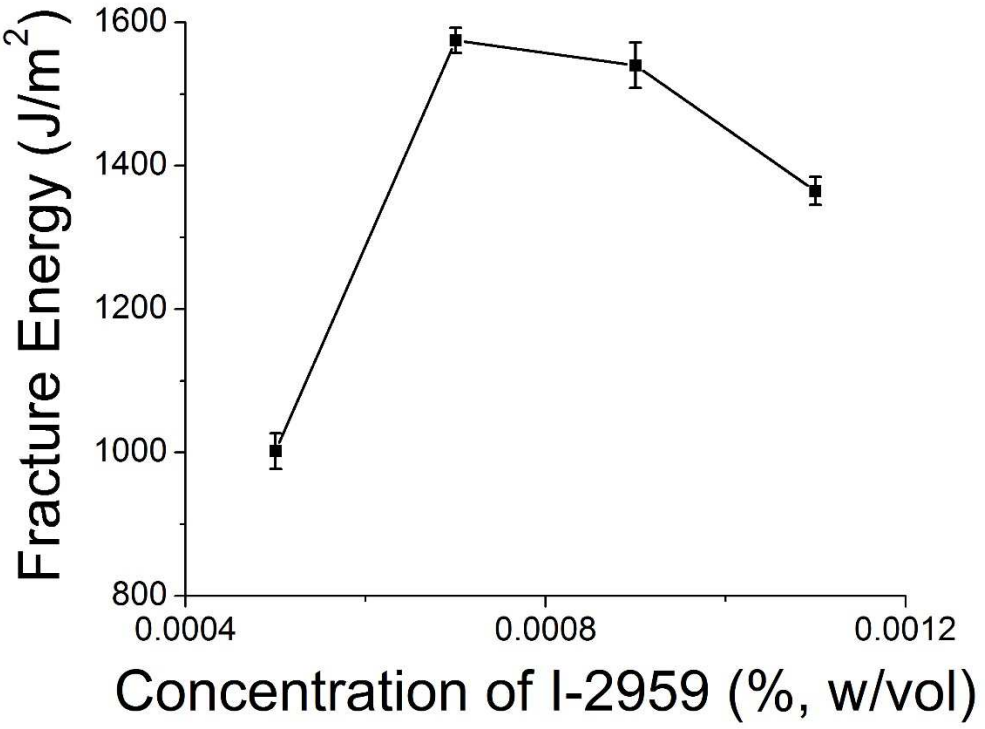

Figure S4. The effect of I-2959 concentration on fracture energy of the hydrogel

Digital image correlation to measure the strain field of the deformed hydrogel

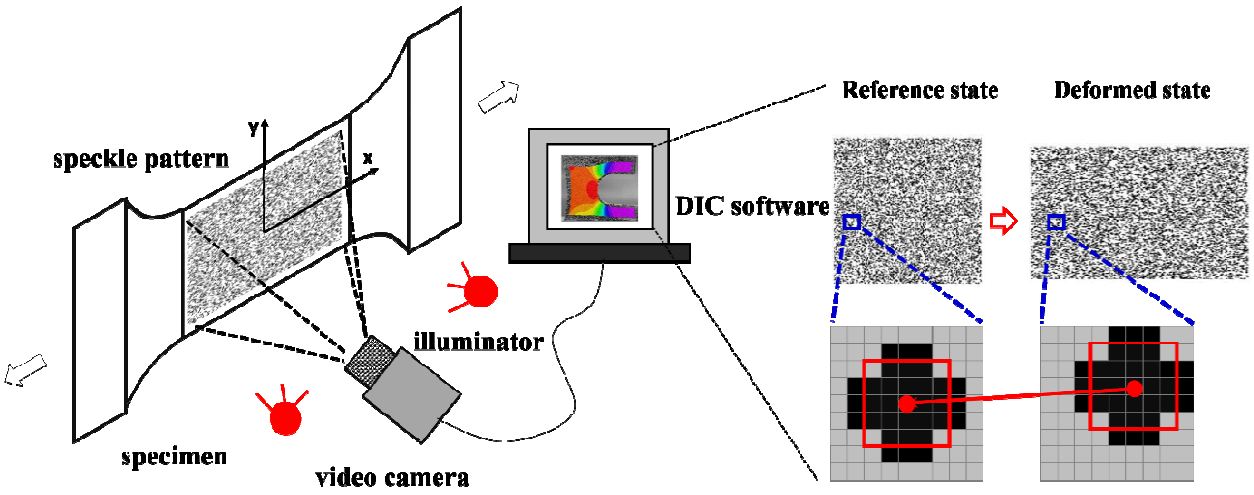

Figure S5. Schematic illustrating the digital image correlation technique. A random speckle pattern was spray painted onto the surface of a sample. Images of the speckle patterns at both the reference state and deformed state were recorded by a standard video camera throughout sample extension. The surface strain was measured by matching the digitalized images before and after deformation via VIC-2D software.

Viscosity of pre-gel solutions with various concentrations of nanoclay

The viscosity of pre-gel solutions with various concentrations of nanoclay was tested in an AR G2, 2° cone and plate viscometer (TA Instruments, New Castle, DE). Each sample was tested in a shear ramp test running from $0.01s^{-1}$ through $100s^{-1}$ shear rate over the course of two minutes. At low shear rates, increasing the concentration of clay as well as adding 50µl of 1M Ca^{2+} per mL of pre-gel solution raises the viscosity; this allows the printed pre-gels to maintain their shapes before the PEGDA is crosslinked. The hydrogel begins to shear thin at a critical shear rate; this results in an inverse relationship between viscosity and shear rate.

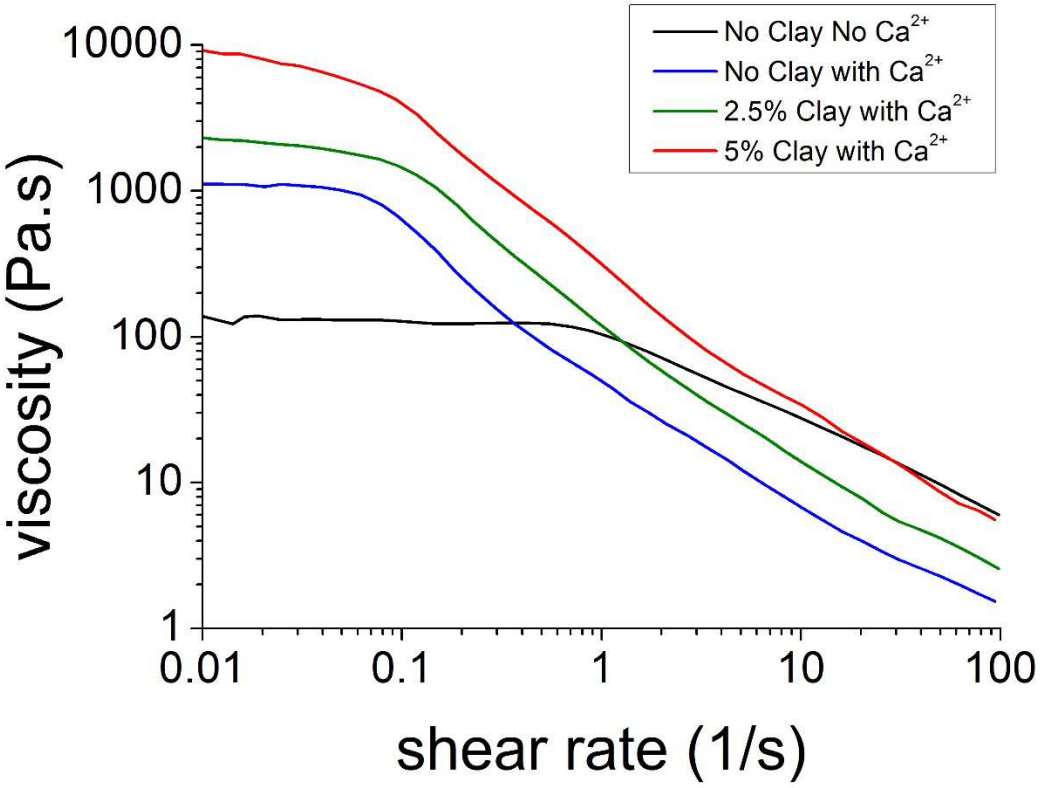

Figure S6. Viscosity of the pre-gel solution with various concentrations of nanoclay as a function of shear rate.

Printed mesh of PEG-alginate-nanoclay hydrogel immersed in collagen

A printed mesh consisting of the previously described PEG-alginate-nanoclay hydrogel was immersed in a cell-laden (HEK cells) collagenous solution. The collagen infiltrates into the mesh of the PEG-alginate-nanoclay hydrogel. At 22 °C, the collagen solution gelled over the course of 20 minutes to form a composite hydrogel composed of collagen gel between the channels of the printed PEG-alginate-nanoclay mesh, as shown below in **Figure S7**. Cell viability in the collagen remained approximately 95% throughout a 7 day study, as shown in Figure 4c.

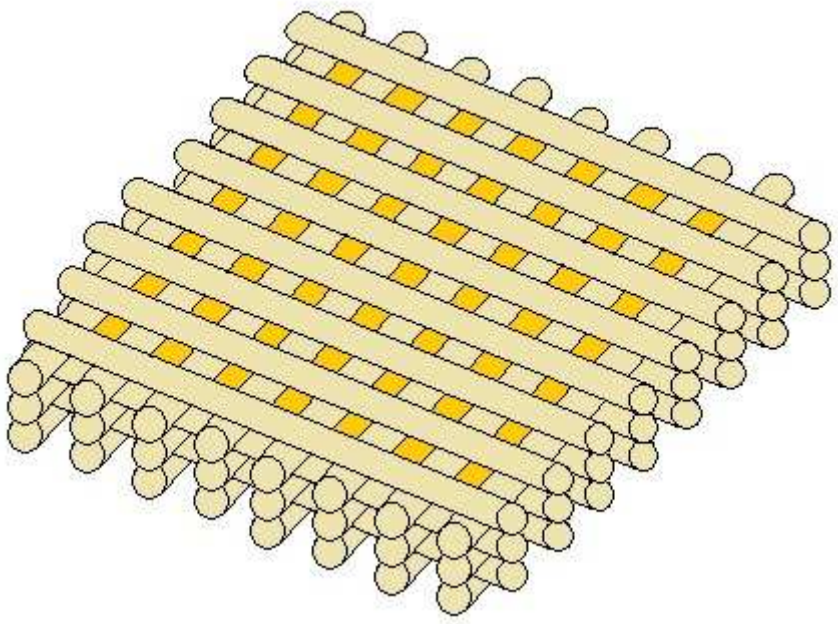

Figure S7. An illustration of a 3D printed PEG-alginate-nanoclay hydrogel mesh (shown above in tan) with collagen gel (gold) formed throughout the interconnected pore network.

Supplementary Movie 1. This movie shows a direct fabrication of a 3D hydrogel cube without the need for support material or post-processing modifications.

Supplementary Movie 2. This movie demonstrates recovery of a printed pyramid of the PEG-alginate hydrogel from compression test. It could withstand 99% compressive strain and nearly recover its original shape when the strain was released.